Topological classification of quasiperiodically driven quantum systems

P. J. D. Crowley,[1,*] I. Martin,[2] and A. Chandran[1]

[1]*Department of Physics, Boston University, Boston, Massachusetts 02215, USA*
[2]*Materials Science Division, Argonne National Laboratory, Argonne, Illinois 60439, USA*

Few-level quantum systems driven by n_f incommensurate fundamental frequencies exhibit temporal analogs of noninteracting phenomena in n_f spatial dimensions, a consequence of the generalization of Floquet theory in frequency space. We organize the fundamental solutions of the frequency lattice model for $n_f = 2$ into a quasienergy band structure and show that every band is classified by an integer Chern number. In the trivial class, all bands have zero Chern number and the quasiperiodic dynamics is qualitatively similar to Floquet dynamics. The topological class with nonzero Chern bands has dramatic dynamical signatures, including the pumping of energy from one drive to the other, chaotic sensitivity to initial conditions, and aperiodic time dynamics of expectation values. The topological class is however unstable to generic perturbations due to exact level crossings in the quasienergy spectrum. Nevertheless, using the case study of a spin in a quasiperiodically varying magnetic field, we show that topological class can be realized at low frequencies as a prethermal phase, and at finite frequencies using counterdiabatic tools.

I. INTRODUCTION

External time-dependent drives are indispensable to a quantum mechanic. At weak amplitude, they probe linear response [1], while at strong amplitude, they enable Hamiltonian engineering [2–27].

The frequency content of the drive determines the nature of the steady state in a few-level quantum system. When the drive has a single fundamental frequency, the Floquet theorem guarantees that observables vary quasiperiodically in time [28,29], while a stochastic drive leads to stochastic behavior.

Recent advances in the construction and control of long-lived coherent qubits in a variety of condensed matter and quantum optical systems allow access to the interesting intermediate regime where the drive has a finite number n_f of incommensurate frequencies [30–40]. Despite the lack of periodicity, the Floquet formalism can be generalized by treating the phase angle associated with each incommensurate frequency as an independent variable. The fundamental solutions of the Schrödinger equation, the so-called quasienergy states, then follow from the solutions of a tight-binding model in n_f independent synthetic dimensions in frequency space [41–43].

Martin *et al.* [43] recently exploited the synthetic dimensions to engineer energy pumping in the adiabatic regime. Specifically, Ref. [43] studied a spin-1/2 in a magnetic field composed of two incommensurate frequencies $\vec{\Omega} = (\Omega_1, \Omega_2)$:

$$H_{\mathrm{CI}}(t) = \vec{B}(t) \cdot \vec{\sigma}, \tag{1}$$

where

$$\vec{B}(t) = \begin{pmatrix} \sin(\Omega_1 t + \theta_{01}) \\ \sin(\Omega_2 t + \theta_{02}) \\ m - \cos(\Omega_1 t + \theta_{01}) - \cos(\Omega_2 t + \theta_{02}) \end{pmatrix}.$$

Interpreting $\Omega_1 t$ and $\Omega_2 t$ as momenta, H_{CI} is the momentum-space Hamiltonian of a two-dimensional Chern insulator (CI) for $0 < |m| < 2$ [44,45]. The Hall response of the Chern insulator at weak electric field translates to the quantized pumping of energy between the drives in the spin problem. In contrast, when $|m| > 2$, the insulator has no Hall response and the spin dynamics qualitatively resemble that of the one-tone case.

Could a different choice of driving Hamiltonian produce more exotic dynamics of the driven spin? We present an exhaustive classification of the quasienergy states of a d-level quantum system (qudit) driven by $n_f = 2$ incommensurate frequencies. The generalized Floquet formalism (Sec. III) produces d fundamental solutions of the Schrödinger equation:

$$|\psi_j(t)\rangle = e^{-i\epsilon_j(\vec{\theta}_0)t} |\phi^j(\vec{\Omega}t + \vec{\theta}_0)\rangle, \tag{2}$$

where $j = 1 \cdots d$, $\epsilon_j(\vec{\theta}_0)$ is a quasienergy and $|\phi^j(\vec{\Omega}t + \vec{\theta}_0)\rangle$ is the associated quasienergy state, which is periodic in both of its arguments. The initial drive phases, $\vec{\theta}_0 \in [0, 2\pi)^2$, define the *Floquet zone*. The quasienergies and states can be organized into a two-dimensional *quasienergy band structure* with d bands over the Floquet zone. The dynamical classes of the driven qudit are indexed by the d integer Chern numbers C_j associated with the bands. We refer to the class with all $C_j = 0$ as trivial and any other class as topological.

Remarkably, the dispersion of band j is fixed by its Chern number:

$$\nabla_{\vec{\theta}_0} \epsilon_j = \frac{C_j}{2\pi}(-\Omega_2, \Omega_1). \tag{3}$$

*philip.jd.crowley@gmail.com

We derive this result in Sec. IV. Heuristically, in the frequency-space tight-binding model $\vec{\Omega}$ plays the role of an electric field which Stark-localizes the quasienergy states in the $\vec{\Omega}$ direction. In the perpendicular direction $\vec{P} = (-\Omega_2, \Omega_1)$, the states are localized if $C_j = 0$ and delocalized otherwise. Varying $\vec{\theta}_0$ twists the phase in the $\vec{P}$ direction; only the delocalized eigenstates respond and move along the electric field direction. Equation (3) quantifies the change in the quasienergy due to the component of the translation in the direction of the electric field.

Equation (3) leads to stark differences in the dynamics starting from generic initial states for the topological and trivial dynamical classes (Sec. V). The topological class is characterized by the pumping of energy between the drives, strong sensitivity to the initial phases of the drives, and aperiodic dynamics of expectation values. The latter two properties are properties of a *quantum chaotic* qudit. In contrast, the trivial class exhibits the same qualitative features as the periodically driven qudit: quasiperiodic dynamics with no energy pumping or chaos. The sensitivity to the initial phase $\vec{\theta}_0$ is due to dephasing between the quasienergy states which produces a linear-in-time divergence of expectation values. We believe that the distance diverges exponentially with a well-defined Lyapunov exponent if the external drive amplitudes are treated as dynamical variables.

In the topological class, the quasienergy band structures contain exact level crossings. In the strict adiabatic limit the Chern indices are stable to Hamiltonian perturbations as they are inherited from a band insulator. At finite frequency, however, the level crossings are unstable to generic perturbations. Using the Chern insulator model in (1) as an example, we demonstrate that the topological class nevertheless controls (i) the prethermal dynamics in the vicinity of the adiabatic limit, and (ii) the dynamics for finite-frequency drives with counterdiabatic terms (Sec. VI). We explicitly construct a counterdiabatic term $V(t)$ with finite spectral bandwidth that ensures that the quasienergy states of

$$H_{\mathrm{CD}}(t) = H_{\mathrm{CI}}(t) + V(t) \tag{4}$$

are given by the instantaneous eigenstates of $H_{\mathrm{CI}}(t)$. Counterdiabatic (CD) terms stabilize the dynamical class of any adiabatic Hamiltonian $H(t)$ at finite drive frequency, and offer a route to realizing the topological class in the laboratory [46,47].

Incommensurate external drives have been previously studied [48–50] including to engineer the Anderson metal-insulator transition in kicked rotors [51,52]. Previous studies have also discovered quasiperiodic and chaotic dynamical regimes in qudits driven by quasiperiodic sequences [53–58], and classified the quasienergy states in terms of their monodromy [54,55]. Our classification in terms of band structures demonstrates completeness, generalizes to any number of tones, connects the dispersion to the Chern number, and derives dynamical properties of the dynamical classes. Using the counterdiabatic prescription, we also derive finite-frequency quasiperiodically driven spin models in the topological class.

II. SETUP AND HAMILTONIAN

Consider a d-level quantum system driven by two ideal classical drives with fundamental frequencies Ω_1 and Ω_2 (Fig. 1). Each drive is a 2π-periodic function of its phase angle. The phase angle θ_{ti} of drive i increases linearly in time:

$$\theta_{ti} = \Omega_i t + \theta_{0i}, \quad i = 1, 2, \tag{5}$$

or more succinctly, $\vec{\theta}_t = \vec{\Omega}t + \vec{\theta}_0$. The vector $\vec{\theta}_0$ sets the *initial drive phases* at $t = 0$.

The Hamiltonian of the two-tone driven system is a 2π-periodic function of each component of $\vec{\theta}_t$. It is therefore conveniently represented in Fourier series:

$$H(\vec{\theta}_t) = \sum_{\vec{n}} H_{\vec{n}} e^{-i\vec{n}\cdot\vec{\theta}_t}, \tag{6}$$

with $\vec{n} = (n_1, n_2) \in \mathbb{Z}^2$.

The drive is quasiperiodic (or equivalently the frequencies Ω_1 and Ω_2 are incommensurate) if and only if Ω_1 and Ω_2 are rationally independent:

$$\Omega_2/\Omega_1 \equiv \beta \notin \mathbb{Q}. \tag{7}$$

In what follows, we use the terms quasiperiodic and incommensurate interchangeably and fix $\beta = (1 + \sqrt{5})/2$ to be the golden ratio.

Rational approximation

Determining whether two drive frequencies are quasiperiodically related requires infinite precision. We expect the finite-time dynamics of the qudit to be insensitive to this property. The quasiperiodic case can therefore be approached through a limiting sequence of rationally (or commensurately) related drives:

$$p\Omega_1 = q\Omega_2. \tag{8}$$

Here p, q are coprime integers determined by the best rational approximations to β. The theory of Diophantine approximation defines the series of *best rational approximations* p/q to the irrational β as the coprime integers p, q such that $|\beta - p/q|$ cannot be made smaller without increasing q. In the *incommensurate limit*, in which q is allowed to be arbitrarily
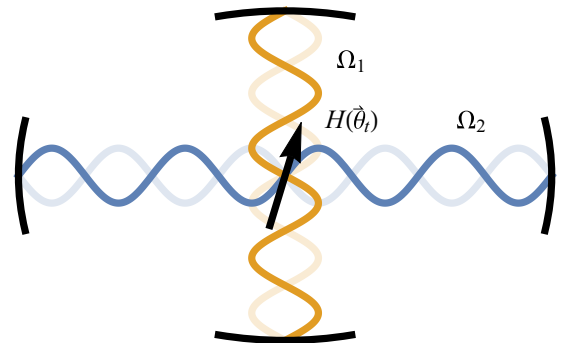

FIG. 1. Two-tone driven quantum systems. A d-level quantum system with Hamiltonian $H(\vec{\theta}_t)$ is driven by two classical cavity modes with frequencies Ω_1 and Ω_2.

large, one then finds $p/q \to \beta$ [59,60]. The commensurate system is periodic with period $T = qT_1 = pT_2$ where $T_i = 2\pi/\Omega_i$. On timescales $t \ll T$, we expect all observables to be the same as in the incommensurate limit, whereas on timescales $t \gtrsim T$, the periodicity of the system becomes important and the dynamics are described by Floquet theory.

Elementary results in the theory of Diophantine approximation state that [59,60] (i) every irrational number has a unique infinite continued fraction expansion

$$\beta = a_0 + \cfrac{1}{a_1 + \cfrac{1}{a_2 + \cfrac{1}{a_3 + \ldots}}}, \tag{9}$$

and (ii) the best rational approximations p_i/q_i to β are given by truncating the continued fraction expansion at the ith level. For example, the best rational approximations to the golden ratio $\beta = (1 + \sqrt{5})/2$ are given by $p_i/q_i = F_{i+2}/F_{i+1}$, where F_i is the ith Fibonacci number.

III. GENERALIZED FLOQUET THEORY AND THE QUASIENERGY BAND STRUCTURE

Let the state of the qudit at time t be denoted by $|\psi(t; \vec{\theta}_0)\rangle$. This state satisfies the Schrödinger equation:

$$i\partial_t |\psi(t; \vec{\theta}_0)\rangle = H(\vec{\Omega}t + \vec{\theta}_0)|\psi(t; \vec{\theta}_0)\rangle. \tag{10}$$

Below, we discuss the structure of the solutions to (10) in the time and frequency domain by generalizing the Floquet formalism (see [42,43] for related treatments). We show that Fourier-transforming (10) yields a tight-binding model in frequency space in two synthetic dimensions (one for each rationally independent drive frequency). We use the spectrum of this tight-binding model to define the quasienergy band structure.

1. The quasienergy operator and spectrum

Substituting the Fourier transform $|\psi(t; \vec{\theta}_0)\rangle = \int d\omega e^{-i\omega t} |\tilde{\psi}(\omega; \vec{\theta}_0)\rangle$ into the Schrödinger equation (10), we obtain

$$\omega|\tilde{\psi}(\omega; \vec{\theta}_0)\rangle = \sum_{\vec{m} \in \mathbb{Z}^2} H_{\vec{m}} e^{-i\vec{m} \cdot \vec{\theta}_0} |\tilde{\psi}(\omega - \vec{m} \cdot \vec{\Omega}; \vec{\theta}_0)\rangle, \tag{11}$$

where the Fourier coefficients $H_{\vec{m}}$ are defined in (6). Equation (11) only couples the frequencies,

$$\omega = \epsilon + \vec{n} \cdot \vec{\Omega}, \tag{12}$$

for $\vec{n} \in \mathbb{Z}^2$ and fixed ϵ. We can therefore find the *fundamental solutions* $|\tilde{\phi}(\omega; \vec{\theta}_0)\rangle$ to (11) which are nonzero only for the frequencies (12). Using the rational independence of Ω_1, Ω_2, we unambiguously label the Fourier components by $\vec{n}$ instead of ω:

$$|\tilde{\phi}_{\vec{n}}(\vec{\theta}_0)\rangle \equiv |\tilde{\phi}(\epsilon + \vec{n} \cdot \vec{\Omega}; \vec{\theta}_0)\rangle. \tag{13}$$

There are multiple solutions of this form corresponding to different values of the quasienergy $\epsilon(\vec{\theta}_0)$. Generic solutions to (11) are linear combinations of the fundamental solutions $|\tilde{\phi}_{\vec{n}}(\vec{\theta}_0)\rangle$ at different $\epsilon(\vec{\theta}_0)$. Combining (11), (12), and (13), we

obtain the eigenvalue equation:

$$\epsilon(\vec{\theta}_0)|\tilde{\phi}_{\vec{n}}(\vec{\theta}_0)\rangle = \sum_{\vec{m}} (H_{\vec{n}-\vec{m}} e^{-i(\vec{n}-\vec{m}) \cdot \vec{\theta}_0} - \vec{n} \cdot \vec{\Omega} \delta_{\vec{n}\vec{m}})|\tilde{\phi}_{\vec{m}}(\vec{\theta}_0)\rangle. \tag{14}$$

We interpret $\vec{n}$ as the lattice sites of a two-dimensional hopping model in frequency space. Explicitly, we define

$$|\tilde{\phi}(\vec{\theta}_0)\rangle = \sum_{\vec{n}} |\tilde{\phi}_{\vec{n}}(\vec{\theta}_0)\rangle \otimes |\vec{n}\rangle, \tag{15}$$

$$K(\vec{\theta}_0) = \sum_{\vec{n}, \vec{m}} [H_{\vec{n}-\vec{m}} e^{-i(\vec{n}-\vec{m}) \cdot \vec{\theta}_0} - \vec{n} \cdot \vec{\Omega} \delta_{\vec{n}\vec{m}}] \otimes |\vec{n}\rangle\langle\vec{m}|, \tag{16}$$

with $\langle\vec{n}|\vec{m}\rangle = \delta_{\vec{n}\vec{m}}$. Then, (14) becomes

$$K(\vec{\theta}_0)|\tilde{\phi}(\vec{\theta}_0)\rangle = \epsilon(\vec{\theta}_0)|\tilde{\phi}(\vec{\theta}_0)\rangle. \tag{17}$$

In analogy to Floquet theory, we refer to ϵ, K, and $|\tilde{\phi}(\vec{\theta}_0)\rangle$ as the quasienergy, the quasienergy operator, and the quasienergy state, respectively. We also define the Floquet zone to be the torus generated by the initial drive phases $\vec{\theta}_0 \in [0, 2\pi)^2$.

2. A tight-binding model in frequency space

We interpret the quasienergy operator K as the Hamiltonian of a two-dimensional tight-binding model using the dictionary in Table I. K consists of (i) an on-site potential $H_{\vec{0}}$, (ii) hopping terms $H_{\vec{n}}$ which couple sites $\vec{m}$ to sites $\vec{m} + \vec{n}$, (iii) an electric field $\vec{\Omega}$ in a non-lattice-vector direction (in the electrostatic gauge), and (iv) a magnetic vector potential $\vec{\theta}_0$. The bulk magnetic field is zero as $\vec{\theta}_0$ is spatially uniform. However, $\vec{\theta}_0$ encodes the twisted boundary conditions of the frequency lattice, as is most easily seen in the commensurate case. For commensurate drives the sites $\vec{n}$ and $\vec{n} + \vec{l}$ correspond to the same frequency in (12), where $\vec{l} = (-p, q)$ is a lattice vector perpendicular to $\vec{\Omega}$. The sites $\vec{n}$ and $\vec{n} + \vec{l}$ should therefore be identified, which compactifies the two-dimensional lattice into a cylinder with circumference $|\vec{l}|$ (see Fig. 2). The cylinder encloses a magnetic flux

$$\Phi = \oint \vec{\theta}_0 \cdot d\vec{r} = \vec{\theta}_0 \cdot \vec{l}. \tag{18}$$

3. The basis of quasienergy states in the time domain

Each distinct solution to the Schrödinger equation (10) in the time domain identifies an equivalence class of quasienergy states on the frequency lattice that are related by lattice translations. This observation resolves the discrepancy between the infinite number of orthonormal solutions on the frequency lattice and the d orthonormal solutions in the time domain.

The quasienergy states in the time domain are obtained by inverse Fourier transform,

$$|\phi^j(t; \vec{\theta}_0)\rangle = \sum_{\vec{n}} e^{-i\vec{n} \cdot \vec{\Omega}t} |\tilde{\phi}_{\vec{n}}^j(\vec{\theta}_0)\rangle, \tag{19}$$

where $j = 1, \ldots d$ labels an orthonormal basis of solutions and $|\tilde{\phi}_{\vec{n}}^j(\vec{\theta}_0)\rangle$ is a representative element of the jth

TABLE I. Dictionary relating quantities in the time and frequency domains.

	Time domain	Frequency domain
$\vec{n}$	Fourier index	Site index
$H_{\vec{0}}$	Time-averaged Hamiltonian	On-site potential
$H_{\vec{m}}$	Fourier component of Hamiltonian	Hopping by vector $\vec{m}$
$\epsilon_j(\vec{\theta}_0)$	Quasienergy	Eigenenergy
$|\tilde{\phi}_{\vec{n}}^j(\vec{\theta}_0)\rangle$	Fourier component of quasienergy state	Quasienergy state projected onto lattice site
$\vec{\Omega}$	Drive frequency vector	Electric field
$\vec{\theta}_0$	Initial drive phase vector	Magnetic vector potential
β	Ratio of drive frequencies $\beta = \Omega_2/\Omega_1$	arctan β is the angle between $\hat{x}$ and $\vec{\Omega}$
d	Hilbert space dimension of qudit	Number of orbitals per lattice site

equivalence class in the frequency lattice. The corresponding solutions to the Schrödinger equation (10) are given by

$$|\psi^j(t)\rangle = e^{-i\epsilon_j(\vec{\theta}_0)t}|\phi^j(t;\vec{\theta}_0)\rangle. \tag{20}$$

To see that quasienergy states related by lattice translations on the frequency lattice correspond to the same solution in the time domain, let $S_{\vec{m}}$ denote the translation by a frequency lattice vector $\vec{m}$: $S_{\vec{m}}|\vec{n}\rangle = |\vec{n}+\vec{m}\rangle$. On conjugation by $S_{\vec{m}}$, K is shifted by a constant

$$S_{\vec{m}} K S_{\vec{m}}^\dagger = K + \vec{m}\cdot\vec{\Omega}. \tag{21}$$

Hence for each quasienergy state $|\tilde{\phi}(\vec{\theta}_0)\rangle$ with quasienergy ϵ, $|\tilde{\phi}'(\vec{\theta}_0)\rangle = S_{\vec{m}}|\tilde{\phi}(\vec{\theta}_0)\rangle$ is a quasienergy state with $\epsilon' = \epsilon + \vec{m}\cdot$
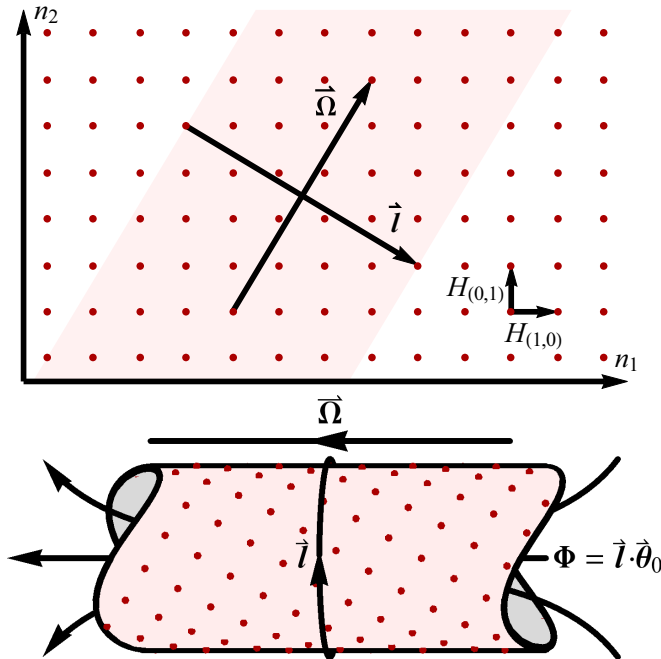

FIG. 2. The frequency lattice. In the incommensurate limit, solutions to Eq. (10) are the solutions of a tight-binding model on an infinite two-dimensional lattice with an electric field $\vec{\Omega}$ (upper panel). The Fourier components $H_{\vec{n}}$ couple sites $\vec{m}$ and $\vec{m}+\vec{n}$ for all $\vec{m}$. When the drive frequencies are commensurate, lattice sites separated by $\vec{l}$ are identified, and the shaded region compactifies into the cylinder shown in the lower panel. This cylinder encloses magnetic flux Φ.

$\vec{\Omega}$. It follows that

$$e^{-i\epsilon t}|\phi(t;\vec{\theta}_0)\rangle = e^{-i\epsilon t}\sum_{\vec{n}} e^{-i\vec{n}\cdot\vec{\Omega}t}|\tilde{\phi}_{\vec{n}}(\vec{\theta}_0)\rangle$$

$$= e^{-i(\epsilon+\vec{m}\cdot\vec{\Omega})t}\sum_{\vec{n}} e^{-i\vec{n}\cdot\vec{\Omega}t}|\tilde{\phi}_{\vec{n}+\vec{m}}(\vec{\theta}_0)\rangle$$

$$= e^{-i\epsilon't}\sum_{\vec{n}} e^{-i\vec{n}\cdot\vec{\Omega}t}|\tilde{\phi}'_{\vec{n}}(\vec{\theta}_0)\rangle$$

$$= e^{-i\epsilon't}|\phi'(t;\vec{\theta}_0)\rangle. \tag{22}$$

Generic solutions $|\psi(t)\rangle$ to the Schrödinger equation (10) are linear combinations of the quasienergy states with their corresponding phases

$$|\psi(t)\rangle = \sum_j \alpha_j e^{-i\epsilon_j(\vec{\theta}_0)t}|\phi^j(t;\vec{\theta}_0)\rangle \tag{23}$$

for constant coefficients $\alpha_j \in \mathbb{C}$.

4. Redundancy of time translations and phase shifts

The Hamiltonian $H(\vec{\theta})$ is invariant under the transformation $t \to t + \tau$, $\vec{\theta}_0 \to \vec{\theta}_0 - \vec{\Omega}\tau$. Thus, $|\phi^j(t;\vec{\theta}_0)\rangle$ and $|\phi^j(t+\tau;\vec{\theta}_0 - \vec{\Omega}\tau)\rangle$ are solutions to the Schrödinger equation at the same quasienergy ϵ_j. Choosing $\tau = -t$ we see that

$$|\phi^j(t;\vec{\theta}_0)\rangle \sim |\phi^j(0;\vec{\theta}_0 + \vec{\Omega}t)\rangle. \tag{24}$$

Above $\sim$ indicates equality up to multiplication by a phase. Equation (24) implies the information encoded by time evolution is also captured by a phase shift.

As the overall phase of a quasienergy state is a gauge choice, i.e., physical observables evaluated in a quasienergy state are invariant under the transformation $|\phi^j(t;\vec{\theta}_0)\rangle \to e^{i\Lambda_j(\vec{\theta}_0)}|\phi^j(t;\vec{\theta}_0)\rangle$, we are free to fix the phase in (24) such that

$$|\phi^j(t;\vec{\theta}_0)\rangle = |\phi^j(0;\vec{\theta}_0 + \vec{\Omega}t)\rangle. \tag{25}$$

Due to the equivalence of time evolution and phase shifts it is then not necessary to keep track of t and $\vec{\theta}_0$ separately. Henceforth we set $t = 0$:

$$|\phi^j(\vec{\theta}_0)\rangle \equiv |\phi^j(0;\vec{\theta}_0)\rangle = \sum_{\vec{n}} |\tilde{\phi}_{\vec{n}}^j(\vec{\theta}_0)\rangle; \tag{26}$$

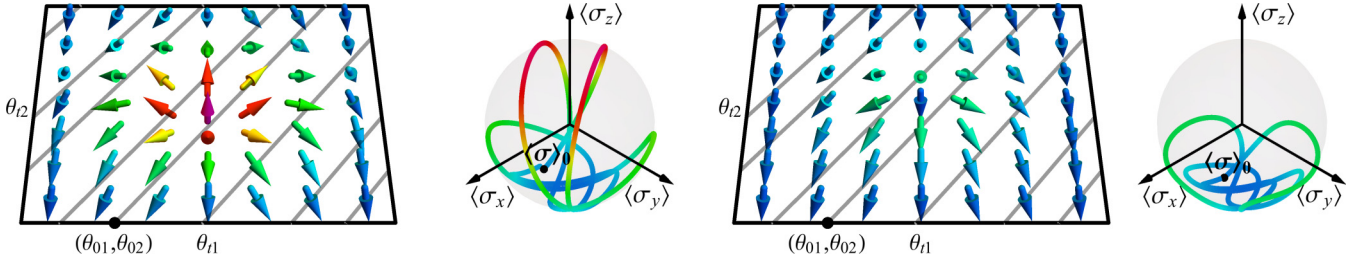$|\phi^j(\vec{\theta}_0)\rangle$ is thus a periodic state defined over the toroidal Floquet zone.

FIG. 3. Visualizing the quasienergy states. The first and third panels show the Bloch vector $\langle \phi^j(\vec{\theta}_t)|\vec{\sigma}|\phi^j(\vec{\theta}_t)\rangle$ of a two-level system throughout the Floquet zone $\vec{\theta}_t \in [0, 2\pi)^2$ for $j = 1$. By (25), the time evolution of a state starting from $\vec{\theta}_0$ corresponds to a straight path through the Floquet zone in the direction $\vec{\Omega}$ (shown in gray for $0 < t < 5T_2$). The second and fourth panels show the path of the Bloch vector on the Bloch sphere in the same interval. The color indicates the z polarization, from blue when $\langle \sigma_z \rangle = -1$ to red when $\langle \sigma_z \rangle = 1$. The left (right) panels illustrate the topological (trivial) dynamical classes, and correspond to quasienergy bands with $C_j = 1$ (0). Data for H_{CD} (67) with $m = 1$ (3) on the left (right), $\vec{\theta}_0 = (-\pi/2, 0)$.

Though this gauge choice may not be smooth, the gauge-invariant properties of $|\phi^j(\vec{\theta}_0)\rangle$ are smooth. For a two-level system, the gauge-invariant properties of the state $|\phi^j(\vec{\theta}_0)\rangle$ are captured by the Bloch vector: $\langle \phi^j(\vec{\theta}_0)|\vec{\sigma}|\phi^j(\vec{\theta}_0)\rangle$, where $\vec{\sigma}$ is the vector of Pauli matrices. These Bloch vector fields are shown in Fig. 3 for the model H_{CI} (1).

5. Quasienergy bands

We promote the index j from labeling the unique solutions at a specific values of $\vec{\theta}_0$ to a band index which labels a state for all $\vec{\theta}_0$.

In the commensurate case with overall period $T = qT_1 = pT_2$ the symmetry (21) implies the band structure $\epsilon(\vec{\theta}_0)$ is invariant under the shift $\epsilon(\vec{\theta}_0) \rightarrow \epsilon'(\vec{\theta}_0) = \epsilon(\vec{\theta}_0) + 2\pi/T$. By choosing the gauge (25) we work in the reduced zone scheme. The reduced zone scheme (pale solid lines in Fig. 4) corresponds to choosing the states with quasienergies $\epsilon(\vec{\theta}_0) \in [-\pi/T, \pi/T]$. These states lie within first "Brillouin zone" (between the horizontal dashed black lines in Fig. 4). In
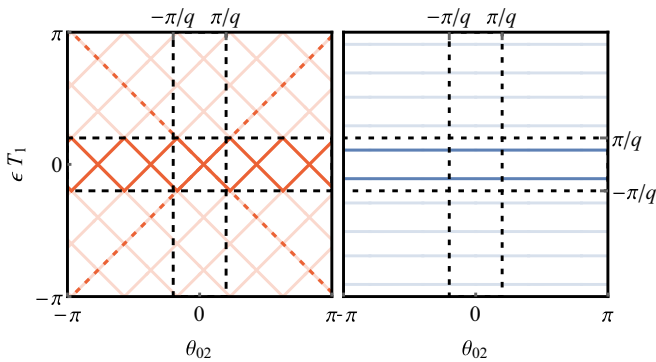

FIG. 4. Band structure of the quasienergy operator. A one-dimensional cut ($\theta_{01} = 0$) of the two-dimensional band structure of the quasienergy operator K for the topological (left) and trivial (right) classes of dynamics in the commensurate approximation. The unbounded spectrum is truncated to $\epsilon_j T_1 \in [-\pi, \pi]$. The solid dark bands are the reduced zone scheme: there is one band with constant positive gradient, and one with constant negative gradient. The dashed dark bands are in the extended zone scheme, while the light bands only appear in the repeated zone scheme. Data from H_{CD} (67) with $(p, q) = (8, 5)$, and $m = 1$ (left), and $m = 3$ (right).

this scheme the quasienergy band structure is invariant under shifts in the time direction $\epsilon(\vec{\Omega}t + \vec{\theta}_0) = \epsilon(\vec{\theta}_0)$; in the $\theta_{01} = 0$ cut shown in Fig. 4 this invariance leads to the corresponding invariance of the quasienergies under the shift $\theta_{02} \rightarrow \theta'_{02} = \theta_{02} + 2\pi/q$. Note however that this symmetry of the quasienergies is not a symmetry of the quasienergy states $|\phi^j(\vec{\theta}_0)\rangle$. In the incommensurate limit $q \rightarrow \infty$ the reduced zone scheme is not well defined as the Brillouin zone $\epsilon \in [-\pi/T, \pi/T]$ collapses; however we will see that properties such as the quasienergy gradient $\nabla_{\vec{\theta}_0} \epsilon(\vec{\theta}_0)$ remain well defined.

The reduced zone scheme is related to the alternative "extended zone scheme" by unfolding (dashed dark lines in Fig. 4); this scheme leads to quasienergies $\epsilon_j(\vec{\theta}_0)$ that are well defined in the quasiperiodic limit, but lacks the useful property $\epsilon(\vec{\Omega}t + \vec{\theta}_0) = \epsilon(\vec{\theta}_0)$. In addition, the repeated zone scheme corresponds to considering the full set of bands (pale solid lines in Fig. 4),

Note that quasienergies $\epsilon_j(\vec{\theta}_0)$ are not ordered by band index in general due to the possibility of exact band crossings (Fig. 4).

IV. TOPOLOGICAL CLASSIFICATION OF QUASIENERGY STATES

The identification of a quasienergy band structure allows us to use the familiar tools of momentum-space band theory to classify the bands. Treating the Floquet zone as the momentum-space Brillouin zone, we immediately see that each band should be characterized by an integer Chern number [61,62]. The Chern number C_j of band j is defined by equating $2\pi C_j$ to the Berry curvature of the quasienergy states $|\phi^j(\vec{\theta}_0)\rangle$ integrated over the Floquet zone.

In static electronic systems, the dispersion is generally not constrained by the Chern number and researchers frequently work with modified Hamiltonians with completely flat energy dispersions [62–64]. Here, we derive the remarkable result that the gradient of the quasienergy dispersion is fixed by the Chern number:

$$\nabla_{\vec{\theta}_0} \epsilon_j(\vec{\theta}_0) = \frac{C_j}{2\pi}(-\Omega_2, \Omega_1). \quad (27)$$

The origin of (27) lies in the response of quasienergy states on the frequency lattice to flux threading. Consider

varying $\vec{\theta}_0$ along the line $\theta_{01} = 0$; Fig. 4 shows band structures along this path in the commensurate case. An increase of θ_{02} by $2\pi/q$ corresponds to a 2π increase of the magnetic flux $\Phi = \vec{\theta}_0 \cdot \vec{l}$ threading the frequency lattice. As a flux of 2π is gauge equivalent to a flux of zero, the quasienergy spectra at θ_{02} and $\theta_{02} + 2\pi/q$ are identical. However, if we follow quasienergy states as we increase θ_{02}, we find that states may exchange positions with one another. Figure 4 shows the two qualitatively distinct possibilities for $d = 2$, $q = 5$. In the left panel, half of the states in the spectrum (pale solid lines) are shifted upon increasing θ_{02} by $2\pi/q$, while the other half are shifted down. Thus, $\Delta\epsilon_j = \pm 2\pi/qT_1 = \pm\Omega_1/q$. In contrast, the spectrum is invariant under arbitrary changes of θ_{02} in the right panel. As the bands in the left (right) panel have $C_j = \pm 1$ (0), we see that $\Delta\epsilon_j = C_j\Omega_1/q = C_j\Omega_1\Delta\theta_{02}/2\pi$. In the incommensurate limit, $q \to \infty$ and we obtain the gradient form in Eq. (27).

Mathematically, the total change in quasienergy of a band on increasing θ_{02} by $2\pi/q$ is given by

$$\Delta\epsilon_j = \int_0^{2\pi/q} d\theta_{02} \frac{\partial\epsilon_j}{\partial\theta_{02}}. \quad (28)$$

We pick a band labeling scheme such that $|\phi^j(\vec{\theta}_0)\rangle$ and $\epsilon_j(\vec{\theta}_0)$ are continuous functions of $\vec{\theta}_0$. From the eigenvalue equation (17), we obtain

$$\nabla_{\vec{\theta}_0}\epsilon_j(\vec{\theta}_0) = \langle\tilde{\phi}^j(\vec{\theta}_0)|[\nabla_{\vec{\theta}_0}K(\vec{\theta}_0)]|\tilde{\phi}^j(\vec{\theta}_0)\rangle. \quad (29)$$

As derived in the Supplemental Material [65], elementary Fourier analysis yields

$$\frac{\partial\epsilon_j}{\partial\theta_{02}} = \langle\tilde{\phi}^j(\vec{\theta}_0)|[\partial_{\theta_{02}}K(\vec{\theta}_0)]|\tilde{\phi}^j(\vec{\theta}_0)\rangle$$
$$= \lim_{t\to\infty}\frac{1}{t}\int_0^t ds\langle\phi^j(\vec{\theta}_s)|[\partial_{\theta_{02}}H(\vec{\theta}_s)]|\phi^j(\vec{\theta}_s)\rangle. \quad (30)$$

The double integral obtained from (30) and (28) provides a uniformly weighted integration over the Floquet zone $0 \leqslant \theta_1, \theta_2 < 2\pi$. Thus

$$\Delta\epsilon_j = \frac{1}{2\pi q}\int_{FZ} d^2\vec{\theta}\langle\phi^j(\vec{\theta})|[\partial_{\theta_2}H(\vec{\theta})]|\phi^j(\vec{\theta})\rangle. \quad (31)$$

Integrating by parts gives

$$\Delta\epsilon_j = -\frac{1}{2\pi q}\int_{FZ} d^2\theta[\langle\partial_{\theta_2}\phi^j(\vec{\theta})|H(\vec{\theta})|\phi^j(\vec{\theta})\rangle + \text{H.c.}]. \quad (32)$$

Next we use the relation

$$i\vec{\Omega}\cdot|\nabla_{\vec{\theta}_0}\phi^j(\vec{\theta}_0)\rangle = [H(\vec{\theta}_0) - \epsilon_j(\vec{\theta}_0)]|\phi^j(\vec{\theta}_0)\rangle, \quad (33)$$

obtained by substituting (20) into the Schrödinger equation (10). Substituting (33) into (32) yields the gauge-invariant result

$$\Delta\epsilon_j = \int_0^{2\pi/q} d\theta_{02} \frac{\partial\epsilon_j}{\partial\theta_{02}} = \frac{\Omega_1 C_j}{q}, \quad (34)$$
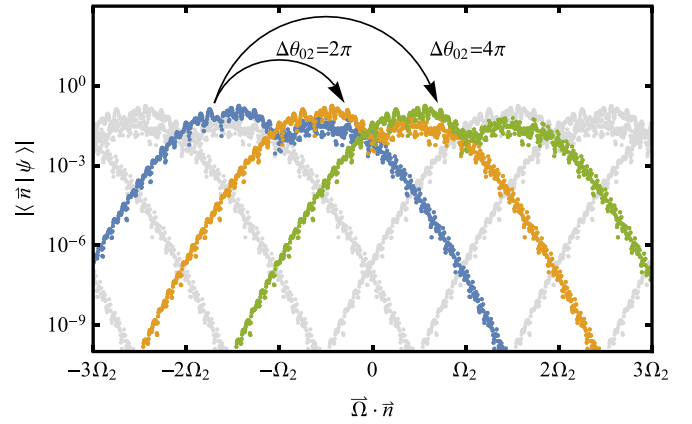

FIG. 5. Shift of quasienergy states on the frequency lattice with flux threading. Amplitudes $|\langle\vec{n}|\psi\rangle|$ of quasienergy states belonging to a band with Chern number $C = 1$ versus the electric potential energy $\vec{\Omega}\cdot\vec{n}$ of the frequency lattice site $\vec{n}$. Threading a 2π flux through the frequency lattice cylinder increases the potential energy of the states and translates them along the electric field. The highlighted states separated by $\Delta\vec{n} = (1,0), (2,0)$ are related by flux changes of $\Delta\theta_{02} = 2\pi, 4\pi$, respectively. Data from H_{CD} (67) with $(p,q) = (34, 21)$, $\Omega_1 = 2\pi/20$, and $m = 1$.

where C_j is the Chern number:

$$C_j = \frac{1}{2\pi i}\int_{FZ} d^2\theta[\langle\partial_{\theta_2}\phi^j|\partial_{\theta_1}\phi^j\rangle - \langle\partial_{\theta_1}\phi^j|\partial_{\theta_2}\phi^j\rangle]. \quad (35)$$

For a two-level system C_j counts the integer number of topological solitons in the Bloch vector field $\langle\phi^j(\vec{\theta}_0)|\vec{\sigma}|\phi^j(\vec{\theta}_0)\rangle$. Examples are shown for the topological and trivial cases in Fig. 3.

In the incommensurate limit, we require that the first derivative of the quasienergy exists. This allows for the identification

$$\frac{\partial\epsilon_j}{\partial\theta_{02}} = \lim_{\Delta\theta_{02}\to 0}\frac{\Delta\epsilon_j}{\Delta\theta_{02}} = \lim_{q\to\infty}\frac{q\Delta\epsilon_j}{2\pi} = \frac{\Omega_1 C_j}{2\pi}. \quad (36)$$

Repeating the above derivation for an increase of θ_{01} by $2\pi/p$ yields the full relation (27).

When the Chern number of a band is nonzero, the quasienergy states are translated by a lattice vector $\vec{m}$ on threading a flux of 2π through the frequency lattice cylinder (see Fig. 5). The vector $\vec{m}$ can be uniquely determined from the change in quasienergy $\Delta\epsilon_j$. For example, increasing θ_{02} by 2π increases the quasienergy of band j by $\Omega_1 C_j$. Using (21), we equate this change to $\vec{m}\cdot\vec{\Omega}$ to obtain $\vec{m} = (C_j, 0)$.

Finally, the quasienergy states $|\phi^j(\vec{\theta}_0)\rangle$ form a complete basis. It follows that the sum of Chern numbers of all the bands is zero at every q:

$$\sum_{j=1}^d C_j = 0. \quad (37)$$

Relation of the Chern number to monodromy

Previous works [54,55] have classified the quasienergy states of incommensurately driven systems by their monodromy. As a trivial monodromy is equivalent to a trivial

Chern number $C_j = 0$ [66], the two classifications are equivalent. For completeness, we briefly discuss the equivalence below.

The quasienergy states belonging to band j have trivial monodromy if and only if there exists a smooth choice of gauge $|\phi_M^j(0, \theta_{02})\rangle \sim |\phi^j(0, \theta_{02})\rangle$ such that the following relation holds:

$$U(T_1, 0; 0, \theta_{02})|\phi_M^j(0, \theta_{02})\rangle = e^{-i\lambda T_1}|\phi_M^j(0, \theta_{02} + 2\pi\beta)\rangle. \tag{38}$$

Above, $\sim$ indicates equality up to a θ_{02}-dependent phase, λ is a constant independent of θ_{02}, and U is the time evolution operator:

$$U(t', t; \vec{\theta}_0) = \mathcal{T} \exp\left[-i\int_t^{t'} ds H(\vec{\Omega}s + \vec{\theta}_0)\right]. \tag{39}$$

Assume that (38) holds. We use time evolution to smoothly extend the definition of $|\phi_M^j\rangle$ to the full Floquet zone:

$$\left|\phi_M^j(\Omega_1 t, \Omega_2 t + \theta_{02})\right\rangle = e^{i\lambda t}U(t, 0; 0, \theta_{02})\left|\phi_M^j(0, \theta_{02})\right\rangle. \tag{40}$$

Using the definition (40) then (38) implies that $|\phi_M^j(2\pi, \Omega_2 T_1 + \theta_{02})\rangle = |\phi_M^j(0, \Omega_2 T_1 + \theta_{02})\rangle$. Thus, $|\phi_M^j\rangle$ is a smooth function of the Floquet zone. By the Stokes theorem, the integrated Berry curvature in (35) is zero. Thus, $C_j = 0$.

If $C_j = 0$, then, ϵ_j is independent of $\vec{\theta}_0$, and the quasienergy state gauge $|\phi^j(0, \theta_2)\rangle$ in the gauge (25) satisfies (38) with $\lambda = \epsilon_j$. We show in the Supplemental Material [65] that this is a smooth gauge, and how to transform to it from any other initial smooth gauge $|\phi_S^j(\vec{\theta}_0)\rangle$ which can be trivially constructed. Thus $C_j = 0$ implies monodromy.

V. DYNAMICAL SIGNATURES OF THE TOPOLOGICAL CLASS

A quasienergy band with a nonzero Chern number has striking dynamical consequences. Qudits in the topological class pump energy between the drives, are sensitive to the initial phases, and have operator expectation values with dense Fourier spectra. Qudits in the trivial class exhibit none of these properties; see Table II. Below, we derive these dynamical
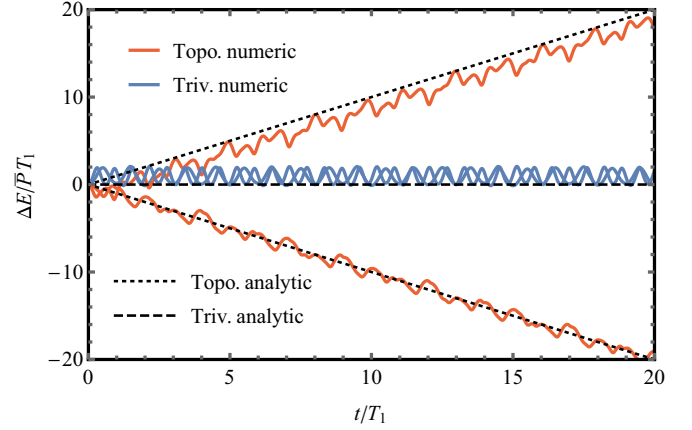

FIG. 6. Energy pumping in quasienergy states. The scaled energy transfer between the two drives as a function of time in the topological (red) and trivial (blue) case for a two-level system prepared in a quasienergy state. Asymptotically, the numerical curves are described by the relation $\Delta E = P_j t$ (black lines). Data from H_{CD} (67) with $m = 1$ (red) and $m = 3$ (blue).

consequences and illustrate them with plots for the model discussed in Sec. VI B.

A. Energy pumping

Reference [43] used an analogy with lattice Chern insulators to argue for quantized energy pumping in quasienergy states in the adiabatic limit. In the adiabatic limit, the electric field $\vec{\Omega}$ in the frequency lattice is weak (Table I). Suppose the model on the frequency lattice at $\vec{\Omega} = 0$ is a Chern insulator. At weak fields, the insulator exhibits the quantum Hall effect; that is, each eigenstate of the frequency lattice carries a quantized current perpendicular to $\vec{\Omega}$. As the components of the site label $\vec{n} = (n_1, n_2)$ on the frequency lattice equal the number of photons in the two drives (up to some arbitrary offset), the Hall effect leads to a quantized rate of transfer of energy between the two drives.

Below, we generalize the argument in Ref. [43] to finite $\vec{\Omega}$ and show that quantized energy pumping is a dynamical signature of quasienergy states in the topological class of dynamics (see Fig. 6).

TABLE II. Properties of the two classes of dynamics for a quasiperiodically driven quantum system.

	Trivial (all $C_j = 0$)	Topological (at least one $C_j \neq 0$)
Gradient of dispersion	$\nabla_{\vec{\theta}_0}\epsilon_j = (0, 0)$	$\nabla_{\vec{\theta}_0}\epsilon_j = \dfrac{C}{2\pi}(-\Omega_2, \Omega_1)$
Sensitivity to perturbation of $\vec{\theta}_0$	Trajectories almost rephase quasiperiodically	Trajectories diverge linearly
Quasienergy states in frequency domain	Localized	Delocalized
Quasienergy states in time domain	Sparse Fourier spectra	Dense Fourier spectra
Frequency lattice response to flux threading	Quasienergy states unchanged	Quasienergy states shift parallel to the electric field
Pump power of band j	$P_j = 0$	$P_j = \dfrac{C_j}{2\pi}\Omega_1\Omega_2$
Floquet operator converges as $U_i \to U(T_i; \vec{\theta}_0)$	Yes	No
Floquet Hamiltonian exists	Yes	No
Time evolution of operator expectation values	Quasiperiodic evolution	Aperiodic evolution

The work done by the second drive up to a time t on a system initially prepared in the quasienergy state is given by

$$\Delta E_j^{(2)}(t) = \int_0^t ds \langle \phi^j(\vec{\theta}_s) | \Omega_2 \partial_{\theta_{02}} H(\vec{\theta}_s) | \phi^j(\vec{\theta}_s) \rangle. \quad (41)$$

The mean rate of work done by the second drive is then

$$P_j^{(2)} = \lim_{t \to \infty} \frac{\Delta E_j^{(2)}(t)}{t}. \quad (42)$$

As the qudit can only contain a finite amount of energy, the rate of work done by each of the two drives on the system must be equal and opposite at long times $P_j^{(1)} = -P_j^{(2)}$. The system therefore behaves as an energy pump with power $P_j^{(1)}$.

Using Eq. (30), we find that the pump power is set by the gradient of the quasienergy dispersion:

$$P_j^{(2)} = \Omega_2 \frac{\partial \epsilon_j}{\partial \theta_{02}}. \quad (43)$$

Equation (27) then provides our result of quantized pumping in the topological class:

$$P_j^{(2)} = -P_j^{(1)} = \frac{C_j}{2\pi} \Omega_1 \Omega_2. \quad (44)$$

Generic initial states (23) also pump energy between the drives. Assuming the quasienergy spectrum is nondegenerate, the contribution of cross terms averages to zero, and the pump power is

$$P_\psi^{(n)} = \sum_j |\alpha_j|^2 P_j^{(n)}, \quad n = 1, 2. \quad (45)$$

We see that $0 \leqslant |P_\psi^{(n)}| \leqslant \max_j |P_j^{(n)}|$. Although the pump power is generically not quantized, it is nonzero except for a measure zero set of states.

In the Chern insulator analogy, the transverse Hall current evaluated in quasienergy states is the photon flux between the drives $\partial_t \langle \vec{n} \rangle$. Using the results derived above,

$$\langle \vec{J} \rangle = \partial_t \langle \vec{n} \rangle = \left(P_j^{(1)}/\Omega_1, P_j^{(2)}/\Omega_2 \right) = \frac{C_j}{2\pi}(-\Omega_2, \Omega_1). \quad (46)$$

We thus recover the quantum Hall effect $\sigma_{xy} = |\vec{\Omega}|/|\langle \vec{J} \rangle| = C_j/2\pi$ in natural units ($e = 1, \hbar = 1$).

B. Divergence of trajectories

Consider two time evolutions starting from the same initial state $|\psi_0\rangle$ but slightly different initial drive phases, $\vec{\theta}_0$ and $\vec{\theta}_0 + \delta\vec{\theta}$. We show the trajectories of the perturbed and unperturbed system asymptotically diverge only in the topological case (see Fig. 7).

The origin of the divergence between trajectories is dephasing in the quasienergy basis. A quasienergy state prepared with initial drive phase vector $\vec{\theta}_0$ evolves as

$$U(t, 0; \vec{\theta}_0) | \phi^j(\vec{\theta}_0) \rangle = e^{-i\epsilon_j(\vec{\theta}_0)t} | \phi^j(\vec{\theta}_t) \rangle, \quad (47)$$

where U is the time evolution operator (39). If we choose a smooth gauge for the states $|\phi^j(\vec{\theta}_0)\rangle$ over the patch $\vec{\theta} \in \vec{\theta}_0 + s\vec{\Omega} + r\delta\vec{\theta}$ for $0 \leqslant s \leqslant t, 0 \leqslant r \leqslant 1$, we can expand the time evolution starting from $\vec{\theta}_0 + \delta\vec{\theta}$ to leading order in $\delta\vec{\theta}$. At leading order, the contribution from expanding $|\phi^j(\vec{\theta}_t + $
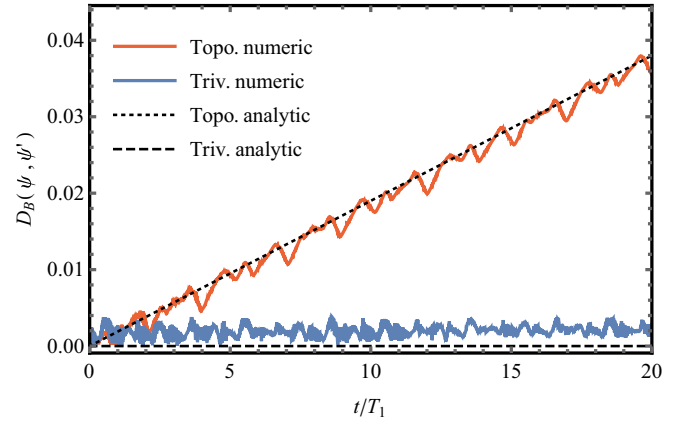

FIG. 7. Divergence of trajectories. In the topological dynamical class, trajectories diverge (red), while the trajectories in the trivial class do not (blue). The asymptotic behavior in Eq. (52) is shown in black. Data from H_{CD} (67) with $m = 1$ (red) and $m = 3$ (blue) for an initial state with $|\alpha_1| = |\alpha_2| = 1/\sqrt{2}$.

$\delta\vec{\theta}\rangle$ is $O(t^0\delta\theta)$, while the term from expanding the phasor $e^{-i\epsilon_j(\vec{\theta}_0 + \delta\vec{\theta})t}$ is $O(t^1\delta\theta)$. In the limit of small $\delta\vec{\theta}$ and large t, therefore, we need only consider the second contribution.

After a time t, the phase difference $e^{i\eta}$ between the states with initial phase vector difference $\delta\vec{\theta}$ is

$$\begin{aligned} \eta &= [\epsilon_j(\vec{\theta}_0 + \delta\vec{\theta}) - \epsilon_j(\vec{\theta}_0)]t + O(\delta\vec{\theta}^2) \\ &= t\delta\vec{\theta} \cdot \nabla_{\vec{\theta}_0} \epsilon_j + O(\delta\vec{\theta}^2) \\ &= \frac{C_j |\vec{\Omega}| \sin\alpha}{2\pi} t |\delta\vec{\theta}| + O(\delta\vec{\theta}^2), \end{aligned} \quad (48)$$

where α is the angle between $\vec{\Omega}$ and $\delta\vec{\theta}$, and we have used (27) [67].

The global phase in (48) is unobservable in pure quasienergy states. As η depends on the band index, (48) leads to dephasing in the quasienergy state basis for generic starting states. To see how the dephasing leads to the divergence of trajectories, consider the evolution from the initial state $|\psi_0\rangle$ with and without the perturbation:

$$\begin{aligned} |\psi_t\rangle &= U(t, 0; \vec{\theta}_0)|\psi_0\rangle, \\ |\psi_t'\rangle &= U(t, 0; \vec{\theta}_0 + \delta\vec{\theta})|\psi_0\rangle. \end{aligned} \quad (49)$$

For concreteness we characterize the distance between the two states using the Bures angle:

$$D_B(\psi, \psi') = \arccos |\langle \psi | \psi' \rangle|. \quad (50)$$

The Bures angle is a distance measure on quantum states [68] and bounds the discriminability of the two states using *any* operator A via the bound

$$|\langle \psi | A | \psi \rangle - \langle \psi' | A | \psi' \rangle| \leqslant 2|A| \sin[D_B(\psi, \psi')], \quad (51)$$

where the operator norm $|A|$ is the magnitude of the leading eigenvalue of A.

For the trivial class of dynamics, the distance $D_B(\psi_t, \psi_t')$ varies quasiperiodically in time and does not grow asymptotically. In contrast, for the topological class, D_B generically grows linearly in time, before saturating at long times to its

maximal value max $D_{\mathrm{B}} = \pi/2$. These results follow from the relation

$$\lim_{t \to \infty} \lim_{|\delta \vec{\theta}| \to 0} \frac{D_{\mathrm{B}}(\psi, \psi')}{t|\delta \vec{\theta}|} = \frac{|\vec{\Omega}| \, \sigma(C) \sin \alpha}{2\pi}. \tag{52}$$

See Supplemental Material [65] for derivation. Above $\sigma(C)$ is the standard deviation of the Chern number in the initial state (23):

$$\sigma^2(C) = \sum_j C_j^2 |\alpha_j|^2 - \left(\sum_j C_j |\alpha_j|^2 \right)^2. \tag{53}$$

Convergence of Floquet unitaries

We have shown that a perturbation to the initial conditions leads to a separation of trajectories for topological dynamics. A perturbation to the drive frequencies Ω_1, Ω_2 can be interpreted as many infinitesimal perturbations to the drive phases. Thus, using the same approach one can show an additional technical consequence of topology: in the trivial class of dynamics this leads to a convergence of the commensurate Floquet unitaries to the incommensurate time evolution operator,

$$\lim_{i \to \infty} |U(q_i T_1, 0; \vec{\theta}_0) - U_i| = 0, \tag{54}$$

whereas in the topological case it does not. Here $U(q_i T_1, 0; \vec{\theta}_0)$ is the time evolution operator (39) in the incommensurate limit $(\Omega_2/\Omega_1 = \beta)$, whereas U_i is the Floquet unitary of the commensurate approximation, found by integrating over the same period with frequencies $\vec{\Omega}'_i = (\Omega_1, \Omega_1 p_i/q_i)$,

$$U_i = \mathcal{T} \exp \left[-i \int_0^{q_i T_1} ds H(\vec{\Omega}'_i s + \vec{\theta}_0) \right]. \tag{55}$$

This can be understood as a perturbation to the second frequency $\Delta\Omega_2 = (p/q - \beta)\Omega_1 \sim 1/q^2$ to the second frequency. For trivial dynamics this convergence can be seen numerically via the corollary of (54),

$$\lim_{i \to \infty} |U_i - (U_{i-1})^{a_i} U_{i-2}| = 0, \tag{56}$$

where a_i are the partial quotients defined via the continued fraction expansion of β (9). Equation (56) follows composing the unitaries corresponding to smaller commensurate periods to approximate one of a larger commensurate period and uses the result of Diophantine approximation that $q_i = a_i q_{i-1} + q_{i-2}$. The two terms in (56) correspond to two different closed paths through the Floquet zone; the limit converges if the small difference to the phase angles $\vec{\theta}_t$ between the two paths is inconsequential.

In contrast when accounting for topology we find that due to the effects discussed in Sec. V B the two trajectories accrue phase differently and there is a correction to the phase,

$$\lim_{i \to \infty} |[U_i - (-1)^{a_i C_j}(U_{i-1})^{a_i} U_{i-2}] |\phi^j(\vec{\theta}_0)\rangle| = 0. \tag{57}$$

The convergence relation has an additional sign $(-1)^{a_i C_j}$ which depends on the Chern number C_j of each quasienergy state's subspace. This topological correction to the composition rule of the Floquet unitaries is derived in the Supplemental Material [65].
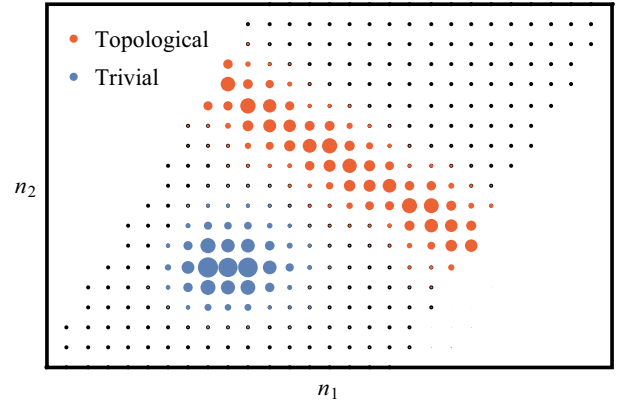

FIG. 8. Localization and delocalization on the frequency lattice. The support of the quasienergy states on the frequency lattice in the commensurate approximation (pink region in Fig. 2). Each red/blue disk is centered on a lattice site $\vec{n}$ and has an area $\propto \ln\langle \tilde{\phi}^j_{\vec{n}}(\vec{\theta}_0) | \tilde{\phi}^j_{\vec{n}}(\vec{\theta}_0) \rangle$. The topological states (red) are delocalized and encircle the cylinder, whereas the trivial states (blue) are localized. Data from H_{CD} (67) with $(p, q) = (8, 5)$, and $m = 1$ (left) and $m = 3$ (right).

C. Delocalization on the frequency lattice and aperiodicity of observables

A quasienergy state $|\tilde{\phi}^j(\vec{\theta}_0)\rangle$ belonging to a band with $C_j \neq 0$ is delocalized on the frequency lattice in the direction perpendicular to the electric field $\vec{\Omega}$. Indeed, in order for the state to be sensitive to flux threading through the cylinder or to pump energy indefinitely, it *has* to be delocalized. See Fig. 8.

As $|\tilde{\phi}^j_{\vec{n}}(\vec{\theta}_0)\rangle$ are the Fourier components of $|\phi^j(\vec{\theta}_t)\rangle$ with frequency $\omega = \epsilon_j + \vec{n} \cdot \vec{\Omega}$, the state $|\phi^j(\vec{\theta}_t)\rangle$ has a dense Fourier spectrum for $C_j \neq 0$. Expectation values are therefore aperiodic in the topological class. If $C_j = 0$, then the quasienergy states are localized on the frequency lattice and the state $|\phi^j(\vec{\theta}_t)\rangle$ has a sparse Fourier spectrum that can be approximated to any desired accuracy with a finite number of components. Expectation values are quasiperiodic in time in this case. See Fig. 9.

VI. STABILITY OF THE TOPOLOGICAL CLASS

The topological class does not extend to a phase because of need of an exact level crossing in the quasienergy band structure. Recall that the Chern numbers satisfy the sum rule $\sum_j C_j = 0$. If there is a band j with $C_j \neq 0$ in the spectrum, then there must be another band j' with a Chern number of the opposite sign by the sum rule. As the Chern number sets the gradient of the dispersion, the bands j and j' must cross. These crossings are visible in Fig. 4. The topological class of dynamics is thus realized only if the quasienergy operator $K(\vec{\theta}_0)$ has exact degeneracies at some $\vec{\theta}_0$. We expect that the exact degeneracy splits upon perturbing $K(\vec{\theta}_0)$. Thus, the topological case is finely tuned, and only the trivial class with all $C_j = 0$ is stable to perturbation.

Despite this generic instability, in this section we study two constructions which realize the topological dynamics in settings amenable to experiment. We start from a model
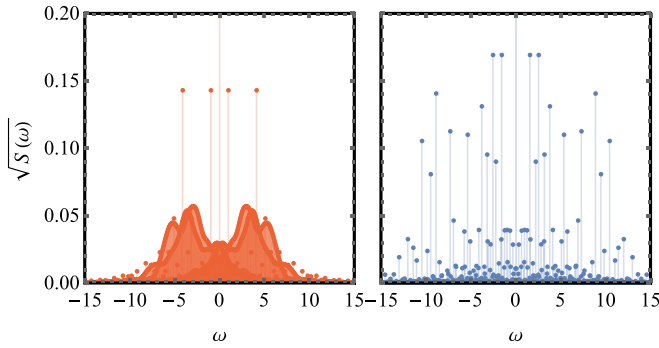
FIG. 9. Spectral properties of expectation values. Square root of the mean power spectrum for topological (left) and trivial (right) classes of dynamics in the commensurate approximation, showing a nascent region of dense spectrum only in the topological case. The power spectrum is averaged over initial states and polarization axes $\vec{a}$ of operators $A = \vec{a} \cdot \vec{\sigma}$ for $|\vec{a}| = 1$. Data from H_{CD} (67) with $(p, q) = (89, 55)$, and $m = 1$ (red) and $m = 3$ (blue).

(introduced in Ref. [43]) which realizes the topological phase exactly in the adiabatic limit. First, we show that at finite drive rate this immediately yields a long prethermal period for which the dynamics of the topological class is observed; second, we use a counterdiabatic correction to produce an explicit, finely tuned model, which realizes the topological class of dynamics indefinitely, at any finite drive rate, and which is exponentially dominated by a finite bandwidth of drive frequencies.

We first consider the Chern insulator (CI) model

$$H_{CI}(\vec{\theta}_t) = \begin{pmatrix} \sin\theta_{t1} \\ \sin\theta_{t2} \\ m - \cos\theta_{t1} - \cos\theta_{t2} \end{pmatrix} \cdot \vec{\sigma} \qquad (58)$$

previously introduced in (1); here $\vec{\sigma} = (\sigma_x, \sigma_y, \sigma_z)$, and $\vec{\theta}_t = \vec{\theta}_0 + \vec{\Omega}t$. We are motivated to study this model by the analogy to Hall physics (see Sec. V A): Eq. (58) is a well-known Chern insulator [44,45] where we have made the replacement $(k_x, k_y) \to (\theta_{t1}, \theta_{t2})$ [69]. It follows that for $0 \leqslant |m| < 2$ the *instantaneous eigenstates* of H_{CI} form bands with nontrivial Chern numbers: $(C_1, C_2) = (1, -1)$ for $0 < m < 2$ which switch signs to $(C_1, C_2) = (-1, 1)$ for $-2 < m < 0$.

In the precise limit $\Omega_1, \Omega_2 \to 0$ it follows from the adiabatic theorem that the quasienergy states are given by the instantaneous eigenstates of H_{CI}, and thus inherit the nontrivial Chern numbers of the Hall problem. These nontrivial Chern numbers constitute a realization of the topological class of dynamics.

A. Prethermal topological dynamics

At finite drive frequencies Ω_1 and Ω_2, the dynamical states of the CI model fail to follow the adiabatic eigenstates, and the system heats by Landau-Zener excitation.

In the low-frequency limit, the Landau-Zener rate of excitation $1/\tau$ is exponentially small in the rate of change of the Hamiltonian [70–73]:

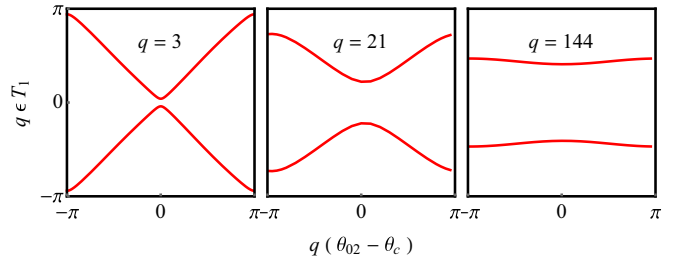$$\ln \tau \sim |\vec{\Omega}|^{-1} \sim T_1, T_2. \qquad (59)$$

FIG. 10. Quasienergy band structure of H_{CI} (58) as the quasiperiodic limit is approached. Plots of quasienergy ϵ_j versus the initial phase $\theta_{02} - \theta_c$, where $\theta_{02} = \theta_c$ is the point of minimum gap. As q increases toward the incommensurate limit, the quasienergy bands flatten. Note the rescaling by q vs Fig. 4. Parameters: $\Omega_1 = 2\pi/15$, $m = 1$.

In the prethermal regime, $0 < t \ll \tau$, this rate is negligible and the deviation from the adiabatic limit is small. A qudit prepared in an instantaneous eigenstate remains close to one, and the dynamics are controlled by the topological class of the strict adiabatic limit. This prethermal regime is exponentially long in the drive period T_1, T_2, making the regime accessible to experiment.

In the commensurate case the total period, $T = qT_1 = pT_2$, provides an additional timescale. In the adiabatic limit the Floquet states of the commensurate problem also have nonzero quasienergy gradient [see (34) and Fig. 4], and so exhibit the properties of the topological class of dynamics. At finite drive rate, if the period $T \ll \tau$ then the effect of Landau-Zener excitation within a period is small, the Floquet states are only weakly perturbed, the quasienergies are close to the quantized values, and the system continues to exhibit the topological dynamics, though the average pumping is no longer quantized. The topological dynamics are exhibited for generic initial conditions except for an exponentially small set of initial conditions close to the avoided crossing of quasienergy bands. For initial conditions close to the avoided crossing the Floquet states are strongly altered, and a state prepared in an instantaneous eigenstate will scatter into other eigenstates on the timescale τ.

The band structure of the commensurate system is depicted in Fig. 10. For $qT_1 \ll \tau$ (left panel) the avoided crossing is small, and for much of the Floquet zone the quasienergy gradient is close to the quantized value (27); from this the dynamical properties of the topological class of dynamics follow. As q is increased, lengthening the period, and bringing the system closer to the incommensurate limit, the avoided crossing begins to dominate the band structure, and the quasienergy levels approach their flat (topologically trivial) limiting form. For $qT_1 \gg \tau$ the signatures of the topological dynamics are lost on the shorter timescale τ.

Energy pumping in the prethermal regime

The Landau-Zener scaling of the loss of the dynamical signatures of the topological class is confirmed by analyzing the energy pumped by the system.

In the Heisenberg picture the instantaneous power of the second drive is given by the operator [see (42), (41)]

$$P^{(2)}(t) = \Omega_2 U^\dagger(t, 0; \vec{\theta}_0) \partial_{\theta_{02}} H(\vec{\theta}_t) U(t, 0; \vec{\theta}_0). \quad (60)$$

The mean power over an interval $[0, t]$ maximized over initial states is then given by

$$P_{\max}^{(2)}(t) = \max_{|\psi_0\rangle} \langle \psi_0| \left[\frac{1}{t} \int_0^t dt' P^{(2)}(t') \right] |\psi_0\rangle. \quad (61)$$

By using this measure we avoid the question of which initial states exhibit pumping most clearly over finite times.

We compare this with the theoretical value for a topological model with Chern number $C = 1$ of $P = \Omega_1 \Omega_2 / 2\pi$ given by (44). Deviation from the topological value is captured by the normalized deviation of the pump power $\bar{P}_j^{(n)}$ from the theoretically maximal value P:

$$\Delta^{(n)}(t) = 1 - \frac{P_{\max}^{(n)}}{P}. \quad (62)$$

In the upper panel of Fig. 11 we plot $\Delta^{(n)}(t)$ vs $\Omega_1 t$ for various values of $T_1 = 2\pi/\Omega_1$ with fixed $\Omega_2/\Omega_1 = (1 + \sqrt{5})/2$. The eventual decay of pumping to zero results in the system converging to asymptotic value $\Delta^{(n)} = 1$ in all cases.

For small times one finds the decay is linear,

$$\Delta^{(n)}(t) = t/\tau + O(t^2/\tau^2). \quad (63)$$

The values of τ are extracted by a linear fit to the data from the upper panel of Fig. 11 in the region $\Delta^{(n)} < 0.6$, i.e., before the curves begin to flatten into their asymptotic values $\Delta^{(n)} = 1$. These extracted values are plotted versus T_1 in the lower panel. We see that the decay time τ is exponentially long in the inverse drive rate,

$$\ln \tau \sim T_1, T_2, \quad (64)$$

consistent with Landau-Zener excitation.

B. Finite-rate counterdiabatic driving

Adding a counterdiabatic correction term to the Hamiltonian prevents the Landau-Zener processes that destroy the dynamical signatures of the topological class on timescales $t \gtrsim \tau$ [46,47]. Using this method we obtain an analytic Hamiltonian that realizes topological dynamics in a quasiperiodically driven system indefinitely. This model has finite frequency bandwidth and finite drive rate, making it amenable to experimental study.

The counterdiabatic correction V precisely cancels the matrix elements coupling the instantaneous eigenstates. For any time-dependent Hamiltonian $H(t)$, the condition for the cancellation is

$$[i\partial_t H + [H, V], H] = 0. \quad (65)$$

For a spin-$1/2$ traceless Hamiltonian, Eq. (65) has the solution

$$V = \frac{i}{2} \frac{[\partial_t H, H]}{\text{tr}[H^2]} + uH + v\mathbf{1} \quad (66)$$

for free parameters u, v. Without loss of generality, we take $u = v = 0$.
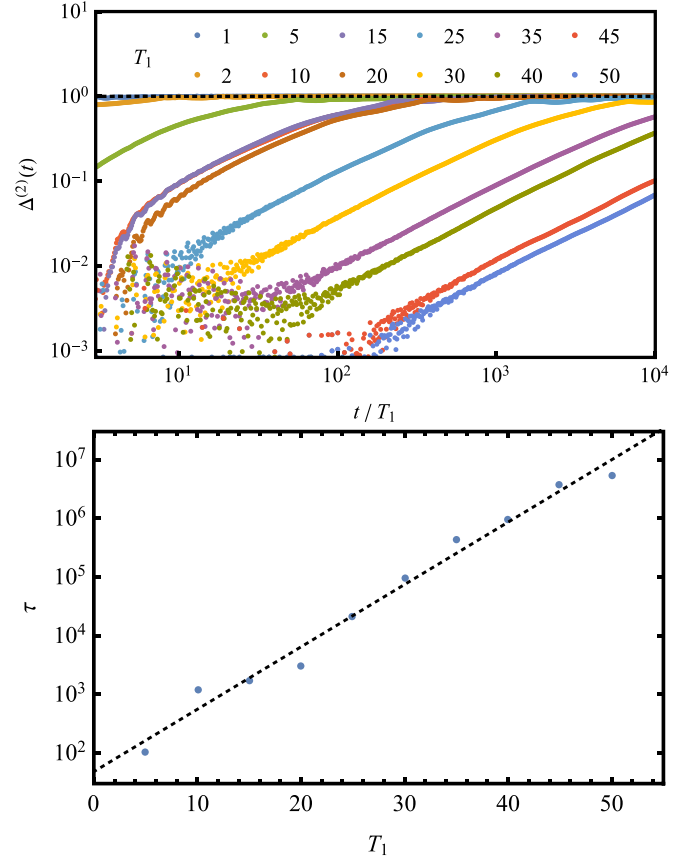

FIG. 11. Decay of quantized pumping in H_{CI} (58). Upper panel: The normalized deviation $\Delta^{(2)}(t)$ [see Eq. (62)] of the time-averaged pump power, maximized over initial states $|\psi_0\rangle$, from the quantized value. At $T_1 < \infty$ (i.e., $\Omega_1, \Omega_2 > 0$) the pumping is found to decay at an initially linear rate which we estimate by fit to each series over the range $10^{-2} < \Delta^{(2)}(t) < 0.4$. Lower panel: This decay rate is exponentially small in the drive rate. Each data point in the upper plot is averaged over $N = 4000$ trajectories with random $\vec{\theta}_0$. Data for model H_{CI} (58) with $m = 1$ and $\vec{\theta}_0$ drawn uniformly from the Floquet zone.

The quasienergy states of the corrected model

$$H_{\text{CD}} = H_{\text{CI}} + V \quad (67)$$

are the instantaneous eigenstates of H_{CI} (58). Thus, if H is in the topological class in the strictly adiabatic limit, then H_{CD} is in the topological class for any drive frequency. The resulting topological quasienergy band structure is verified in Fig. 12 (using the same parameters as in Fig. 10).

The norm of the Fourier amplitudes of H_{CD} for the Chern insulator model is shown in Fig. 13. We see that the norm decays exponentially away from zero frequency. Thus, the corresponding frequency lattice model has exponentially decaying hopping terms. The length scale of the exponential decay is set by the ratio of the energy scales of hopping terms and on-site potential terms in the bare Hamiltonian; precisely one finds (67) has hopping terms $H_{\text{CD},\vec{n}} \sim O(\Delta_{\min}^{|\vec{n}|_1})$ with the minimum gap $\Delta_{\min} = |1 - |1 - |m||$ and $|\vec{n}|_1 = |n_1| + |n_2|$. Thus, approximating H_{CD} by truncating to the N largest Fourier amplitudes leads to an exponentially small
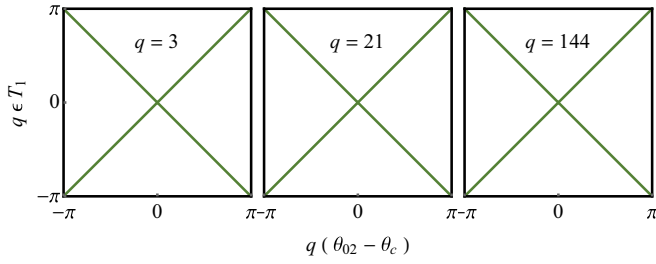
FIG. 12. Quasienergy band structure of H_{CD} (67) as a function of q. The quasienergy ϵ_j versus the initial phase $\theta_{02} - \theta_c$ where $\theta_{02} = \theta_c$ is the point of minimum gap in the extended zone scheme. The counterdiabatic term in (66) protects the linearly dispersing bands and exact level crossings at all q. The dynamical class is topological as $q \to \infty$. Parameters $\Omega_1 = 2\pi/15$, $m = 1$ as in Fig. 10.

in N error term in $H_{\mathrm{CD}}(t)$. This truncation leads to hybridization of the instantaneous eigenstates, as in the previous section. The dynamics of the topological class are then lost after an exponentially long prethermal regime $t \ll \tau$ with $\ln \tau \sim N$.

Numerical observation of the topological class with H_{CD} in the Chern insulator model

We numerically verify that $H_{\mathrm{CD}}(t) = H_{\mathrm{CI}}(t) + V(t)$ realizes the topological class of dynamics for $0 < |m| < 2$ and the trivial class of dynamics for $|m| > 2$.

a. Stable topological band-structure. Figure 4 shows the quasienergy band structure of $H_{\mathrm{CD}}(t)$ at $q = 5$. Without the counterdiabatic correction, the bands flatten with increasing q for any m, as shown in Fig. 10. $V(t)$ protects the exact level crossings for $0 < |m| < 2$ as $q \to \infty$ in Fig. 12, so that the dynamical class is topological in the incommensurate limit.

b. Net energy pumping. The total energy pumped as a function of time is shown in Fig. 6 for the topological (red) and trivial (blue) classes. Asymptotically, both curves follow the theoretical prediction in (44).
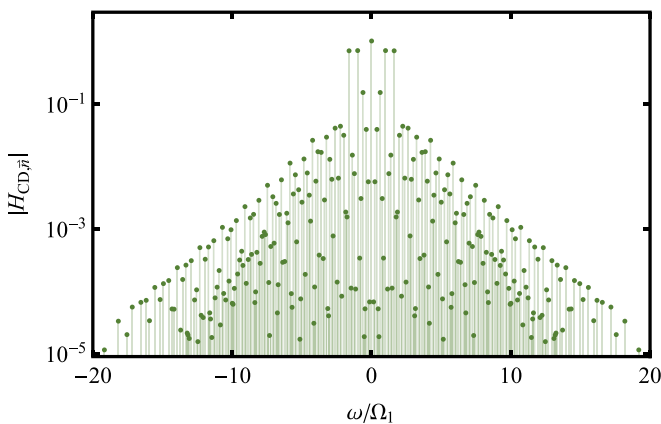
c. Divergence of trajectories. Figure 6 shows the dynamics of the Bures angle (50) for nearby initial states for topological (red) and trivial (blue) dynamics. Asymptotically, both curves follow the theoretical prediction in (52).

d. Delocalization on the frequency lattice. In the topological class, the quasienergy states are delocalized on the frequency lattice (Sec. V C). Figure 8 qualitatively shows this. We show quantitatively (see Supplemental Material [65]) that the scaling in the commensurate limit is consistent with frequency lattice quasienergy states that are delocalized in the topological class and localized in the trivial class.

e. Dense Fourier spectra of observables. The Fourier amplitude $A(\omega)$ of an expectation value $\langle A(t) \rangle$ is given by

$$\langle \psi(t)|A|\psi(t)\rangle = \sum_{j,j'} \sum_{\vec{n},\vec{m}} \alpha_j^* \alpha_{j'} \langle \phi_{\vec{m}}^j |A| \phi_{\vec{n}+\vec{m}}^{j'} \rangle e^{-i(\vec{\Omega}\cdot\vec{n} + \epsilon_{j'} - \epsilon_j)t}$$

$$= \sum_{\omega} A(\omega) e^{-i\omega t}, \tag{68}$$

for some observable A and a generic initial state (23). We characterize the Fourier amplitude by the mean power spectrum

$$S(\omega) = [|A(\omega)|^2]_{A, |\psi_0\rangle} \tag{69}$$

where the right-hand side is averaged over operators of the form $A = \vec{a} \cdot \vec{\sigma}$ with $\vec{a}$ drawn uniformly from the unit sphere, and initial states drawn uniformly from the Bloch sphere. For details of this calculation see the Supplemental Material [65].

$\sqrt{S(\omega)}$ is the root-mean-squared magnitude of the Fourier coefficients of $\langle \psi(t)|A|\psi(t)\rangle$. The values of $\sqrt{S(\omega)}$ are plotted as lollipops for the trivial and topological cases in Fig. 9 using the commensurate approximation. Spectra for the topological and trivial cases are found to have a pure-point part, whereas only the topological case has a continuous part. The nascent continuous part of the topological spectrum is visible in Fig. 9 where the lollipops appear to blur together into lines [74].

We further verify (see Supplemental Material [65]) via scaling in the commensurate approximation that in the quasiperiodic limit, the spectrum $A(\omega)$ becomes dense in the topological class and remains sparse in the trivial class.

VII. SUMMARY AND DISCUSSION

We have classified the dynamical properties of a d-level qu$d$it driven by two tones with incommensurate frequencies using d integer Chern numbers. The generalization of Floquet theory to the two-tone setting identifies a two-dimensional tight-binding model in frequency (Fourier) space; the Hamiltonian of this model is the quasienergy operator K. We organized the eigenstates of K with distinct time dependencies into a quasienergy band structure on the torus of initial drive phases, with integer Chern number C_j associated with each band j.

Starting from a generic initial qudit state, we observe (1) the pumping of energy between the drives, (2) sensitivity to the drive phases at $t = 0$, and (3) aperiodic dynamics of observables, *only* in the topological class (with at least one $C_j \neq 0$). In contrast, the phenomenology of the trivial class (with all $C_j = 0$) is the same as the one-tone driven case.

Although the topological class does not extend to a phase with a finite volume in the parameter space, it leads to an

FIG. 13. Fourier spectrum of H_{CD} (67). The Frobenius norm of the largest 265 Fourier components $H_{\mathrm{CD},\vec{n}}$ of the Hamiltonian H_{CD} [defined via $H_{\mathrm{CD}}(\vec{\theta}_t) = \sum_{\vec{n}} H_{\mathrm{CD},\vec{n}} e^{-i\vec{n}\cdot\vec{\theta}_t}$] for $m = 1$. These are plotted versus their corresponding frequency $\omega = \vec{n}\cdot\vec{\Omega}$. The spectrum is exponentially decaying away from $\omega = 0$ due to the analyticity of H_{CD}.

exponentially long prethermal regime in the near-adiabatic limit. For finite drive frequencies (nonadiabatic regime), we constructed (fine-tuned) models that belong to the topological class using counterdiabatic methods. These correspond to introducing an infinite number of extra hopping elements on the frequency lattice, with magnitude decaying exponentially with the hopping distance.

More generally, the band crossing required to realize the topological class can be accomplished by introducing extra tuning parameters in the Hamiltonian. In the case of counterdiabatic driving the extra parameters are the higher harmonics (which correspond to long-range hops on the frequency lattice). Based on the general theory [75], two-band touching requires tuning of three parameters for a general unitary evolution operator or fewer in the presence of extra symmetry. The number of needed tuning parameters defines the codimension of the band-touching manifold in the full parameter space. Note that if the codimension is greater than one (e.g., a point in 2D, or a line in 3D, both corresponding to codimension two), the manifold cannot split the parameter space into disjoint subspaces, and the band-touching points cannot demarcate the boundaries of distinct trivial phases.

One may also access additional tuning parameters by considering more than two incommensurate drives, $n_f > 2$. In this case, there are $n_f - 1$ independent relative phases, and the quasienergy $\epsilon_j(\vec{\theta}_0)$ is a nontrivial function of $n_f - 1$ variables, facilitating the quasienergy level crossings. The physical significance of such models and possible manifestations of topological phases in this case (analogous to frequency pumping for $n_f = 2$) are open and interesting questions.

Furthermore, in future research it will be interesting to investigate how extra symmetries and extra parameters can be used to access the topological classes. For instance, an analog of time-reversal symmetry at special points in the Floquet zone can lead to Kramers doublets in the quasienergy spectrum, and therefore exact level crossings in the quasienergy band structure. The role of symmetry and its effects on the dynamical classification can be investigated in driven qudit models inspired by the momentum-space representation of the Kane-Mele model [76] or models with a Zak phase [77,78].

Dissipative forces provide another route to stabilize the topological class, as noted in Ref. [43]. If the relaxation time of the qudit is much smaller than the Landau-Zener mixing time (59), then the qudit remains close to the instantaneous ground state indefinitely. The qudit will therefore pump energy between the drives at a nearly quantized rate even at finite drive frequencies if the quasienergy band associated with the instantaneous ground state has a nonzero Chern number. However, such inherently quantum effects as the sensitivity to initial drive phases which rely on phase coherence will be lost. Understanding the effects of different types of dissipative forces on the properties of the topological class is crucial for the experimental observation of the topological class.

Finally, the combination of spatial and synthetic dimensions may result in new dynamical classes with no equilibrium counterpart. Rudner *et al.* [19] followed by Refs. [79–83] developed classifications for the Floquet unitaries of extended systems and showed new topological orders of robust edge modes in periodically driven trivial insulators.

It would be very interesting to extend that framework for incommensurately driven insulators.

ACKNOWLEDGMENTS

[1] D. Forster, *Hydrodynamic Fluctuations, Broken Symmetry, and Correlation Functions*, W. A. Benjamin, Advanced Book Program (Westview Press, 1995).

[2] M. Bukov, L. D'Alessio, and A. Polkovnikov, Adv. Phys. **64**, 139 (2015).

[3] F. Meinert, M. J. Mark, K. Lauber, A. J. Daley, and H.-C. Nägerl, Phys. Rev. Lett. **116**, 205301 (2016).

[4] M. Holthaus, J. Phys. B: At., Mol. Opt. Phys. **49**, 013001 (2015).

[5] K. I. Seetharam, C.-E. Bardyn, N. H. Lindner, M. S. Rudner, and G. Refael, Phys. Rev. B **99**, 014307 (2019).

[6] W. Yao, A. MacDonald, and Q. Niu, Phys. Rev. Lett. **99**, 047401 (2007).

[7] T. Oka and H. Aoki, Phys. Rev. B **79**, 081406 (2009).

[8] J.-i. Inoue and A. Tanaka, Phys. Rev. Lett. **105**, 017401 (2010).

[9] T. Kitagawa, E. Berg, M. Rudner, and E. Demler, Phys. Rev. B **82**, 235114 (2010).

[10] Z. Gu, H. Fertig, D. P. Arovas, and A. Auerbach, Phys. Rev. Lett. **107**, 216601 (2011).

[11] N. H. Lindner, G. Refael, and V. Galitski, Nat. Phys. **7**, 490 (2011).

[12] T. Kitagawa, T. Oka, A. Brataas, L. Fu, and E. Demler, Phys. Rev. B **84**, 235108 (2011).

[13] L. Jiang, T. Kitagawa, J. Alicea, A. Akhmerov, D. Pekker, G. Refael, J. I. Cirac, E. Demler, M. D. Lukin, and P. Zoller, Phys. Rev. Lett. **106**, 220402 (2011).

[14] B. Dóra, J. Cayssol, F. Simon, and R. Moessner, Phys. Rev. Lett. **108**, 056602 (2012).

[15] N. H. Lindner, D. L. Bergman, G. Refael, and V. Galitski, Phys. Rev. B **87**, 235131 (2013).

[16] P. Delplace, Á. Gómez-León, and G. Platero, Phys. Rev. B **88**, 245422 (2013).

[17] Y. T. Katan and D. Podolsky, Phys. Rev. Lett. **110**, 016802 (2013).

[18] T. Iadecola, D. Campbell, C. Chamon, C.-Y. Hou, R. Jackiw, S.-Y. Pi, and S. V. Kusminskiy, Phys. Rev. Lett. **110**, 176603 (2013).

[19] M. S. Rudner, N. H. Lindner, E. Berg, and M. Levin, Phys. Rev. X **3**, 031005 (2013).

[20] J. Cayssol, B. Dóra, F. Simon, and R. Moessner, Phys. Status Solidi RRL **7**, 101 (2013).

[21] M. Lababidi, I. I. Satija, and E. Zhao, Phys. Rev. Lett. **112**, 026805 (2014).

[22] N. Goldman and J. Dalibard, Phys. Rev. X **4**, 031027 (2014).

[23] A. G. Grushin, Á. Gómez-León, and T. Neupert, Phys. Rev. Lett. **112**, 156801 (2014).

[24] A. Kundu, H. A. Fertig, and B. Seradjeh, Phys. Rev. Lett. **113**, 236803 (2014).

[25] J. K. Asbóth, B. Tarasinski, and P. Delplace, Phys. Rev. B **90**, 125143 (2014).

[26] D. Carpentier, P. Delplace, M. Fruchart, and K. Gawędzki, Phys. Rev. Lett. **114**, 106806 (2015).

[27] L. C. Wang, X. P. Li, and C. F. Li, Phys. Rev. B **95**, 104308 (2017).

[28] J. H. Shirley, Phys. Rev. **138**, B979 (1965).

[29] H. Sambe, Phys. Rev. A **7**, 2203 (1973).

[30] J. I. Cirac and P. Zoller, Phys. Today **57**(3), 38 (2004).

[31] F. Jelezko, T. Gaebel, I. Popa, M. Domhan, A. Gruber, and J. Wrachtrup, Phys. Rev. Lett. **93**, 130501 (2004).

[32] M. H. Devoret, A. Wallraff, and J. M. Martinis, arXiv:cond-mat/0411174.

[33] C. Langer, R. Ozeri, J. D. Jost, J. Chiaverini, B. DeMarco, A. Ben-Kish, R. Blakestad, J. Britton, D. Hume, W. M. Itano *et al.*, Phys. Rev. Lett. **95**, 060502 (2005).

[34] J. Taylor, H.-A. Engel, W. Dür, A. Yacoby, C. Marcus, P. Zoller, and M. Lukin, Nat. Phys. **1**, 177 (2005).

[35] B. Trauzettel, D. V. Bulaev, D. Loss, and G. Burkard, Nat. Phys. **3**, 192 (2007).

[36] A. Gali, Phys. Rev. B **79**, 235210 (2009).

[37] R. Blatt and C. F. Roos, Nat. Phys. **8**, 277 (2012).

[38] T. P. Harty, D. T. C. Allcock, C. J. Ballance, L. Guidoni, H. A. Janacek, N. M. Linke, D. N. Stacey, and D. M. Lucas, Phys. Rev. Lett. **113**, 220501 (2014).

[39] G. Wendin, Rep. Prog. Phys. **80**, 106001 (2017).

[40] Y. Wang, M. Um, J. Zhang, S. An, M. Lyu, J.-N. Zhang, L.-M. Duan, D. Yum, and K. Kim, Nat. Photonics **11**, 646 (2017).

[41] T.-S. Ho, S.-I. Chu, and J. V. Tietz, Chem. Phys. Lett. **96**, 464 (1983).

[42] A. Verdeny, J. Puig, and F. Mintert, Z. Naturforsch., A **71**, 897 (2016).

[43] I. Martin, G. Refael, and B. Halperin, Phys. Rev. X **7**, 041008 (2017).

[44] X.-L. Qi, Y.-S. Wu, and S.-C. Zhang, Phys. Rev. B **74**, 085308 (2006).

[45] B. A. Bernevig, T. L. Hughes, and S.-C. Zhang, Science **314**, 1757 (2006).

[46] A. del Campo, Phys. Rev. Lett. **111**, 100502 (2013).

[47] D. Sels and A. Polkovnikov, Proc. Natl. Acad. Sci. U.S.A. **114**, E3909 (2017).

[48] Y. Peng and G. Refael, Phys. Rev. B **97**, 134303 (2018).

[49] Y. Peng and G. Refael, Phys. Rev. B **98**, 220509(R) (2018).

[50] P. T. Dumitrescu, R. Vasseur, and A. C. Potter, Phys. Rev. Lett. **120**, 070602 (2018).

[51] G. Casati, I. Guarneri, and D. Shepelyansky, Phys. Rev. Lett. **62**, 345 (1989).

[52] J. Wang and A. M. Garcia-Garcia, Phys. Rev. E **79**, 036206 (2009).

[53] J. Luck, H. Orland, and U. Smilansky, J. Stat. Phys. **53**, 551 (1988).

[54] H. Jauslin and J. Lebowitz, Chaos **1**, 114 (1991).

[55] P. Blekher, H. Jauslin, and J. Lebowitz, J. Stat. Phys. **68**, 271 (1992).

[56] H. Jauslin and J. Lebowitz, *Mathematical Physics X* (Springer, 1992), pp. 313–316.

[57] J. C. Barata, Rev. Math. Phys. **12**, 25 (2000).

[58] G. Gentile, J. Stat. Phys. **115**, 1605 (2004).

[59] J. W. S. Cassels, *An Introduction to Diophantine Approximation* (Cambridge University Press, Cambridge, 1957).

[60] M. Hindry and J. H. Silverman, *Diophantine Geometry: An Introduction* (Springer Science & Business Media, 2013).

[61] D. J. Thouless, M. Kohmoto, M. P. Nightingale, and M. den Nijs, Phys. Rev. Lett. **49**, 405 (1982).

[62] B. A. Bernevig and T. L. Hughes, *Topological Insulators and Topological Superconductors* (Princeton University Press, 2013).

[63] T. Neupert, L. Santos, C. Chamon, and C. Mudry, Phys. Rev. Lett. **106**, 236804 (2011).

[64] J. McGreevy, B. Swingle, and K.-A. Tran, Phys. Rev. B **85**, 125105 (2012).

[65] See Supplemental Material at http://link.aps.org/supplemental/10.1103/PhysRevB.99.064306 for additional supporting numerics and derivations of Eqs. (30), (52), (69).

[66] M. Stone and P. Goldbart, *Mathematics for Physics: A Guided Tour for Graduate Students* (Cambridge University Press, 2009).

[67] We note that $A = \sin\alpha|\Omega||\delta\theta| t$ is the area in the Floquet zone enclosed by the two perturbed trajectories between the initial perturbation and measurement at time t. Generalizing the argument here one finds that the phase difference between two perturbed quasienergy state trajectories is given by $\eta = \frac{AC_j}{2\pi}$.

[68] Formally this measure is a statistical distance. This entails that the Bures angle has the following properties: Non-negativity $D_B(\psi, \psi') > 0$, symmetry $D_B(\psi, \psi') = D_B(\psi', \psi)$, identity of indiscernibles and $D_B(\psi, \psi) = 0$, and the triangle inequality $D_B(\psi, \psi') \leqslant D_B(\psi, \psi'') + D_B(\psi'', \psi')$.

[69] Note that the quasienergy band structure described in Sec. IV is different from the usual band structure of the model (58) as we have included the nonperturbative effects of the field Ω as opposed to the usual Kubo-formula calculation where the effect of the electric field is accounted for perturbatively.

[70] L. D. Landau, Zur Theorie der Energieübertragung. II **2**, 46 (1932).

[71] C. Zener, Proc. R. Soc. London A **137**, 696 (1932).

[72] E. K. G. Stueckelberg, *Theorie der unelastischen Stösse zwischen Atomen* (Birkhäuser, 1933).

[73] E. Majorana, Il Nuovo Cimento (1924-1942) **9**, 43 (1932).

[74] We note that the topological power spectra are seen here to be comprised of three lines, corresponding to the frequencies $\Omega \cdot n$ and $\Omega \cdot n \pm \omega_{jj'}$ where $\omega_{jj'} = \epsilon_j - \epsilon_{j'}$ is the difference between consecutive quasienergies. In the quasiperiodic limit the separation between the points making up these curves tends to zero, and they cannot be resolved.

[75] J. von Neumann and E. Wigner, Z. Phys. **30**, 467 (1929).

[76] C. L. Kane and E. J. Mele, Phys. Rev. Lett. **95**, 226801 (2005).

[77] J. Zak, Phys. Rev. Lett. **62**, 2747 (1989).

[78] P. Delplace, D. Ullmo, and G. Montambaux, Phys. Rev. B **84**, 195452 (2011).

[79] F. Nathan and M. S. Rudner, New J. Phys. **17**, 125014 (2015).

[80] R. Roy and F. Harper, Phys. Rev. B **94**, 125105 (2016).

[81] D. V. Else and C. Nayak, Phys. Rev. B **93**, 201103 (2016).

[82] A. C. Potter, T. Morimoto, and A. Vishwanath, Phys. Rev. X **6**, 041001 (2016).

[83] R. Roy and F. Harper, Phys. Rev. B **96**, 155118 (2017).